The University of Texas at Austin

Nuclear & Radiation Engineering

Discontinuous Galerkin Finite Elements for Discrete Ordinates Radiation Transport

William L. Gurecky

ME397P

Dr. Derek Haas, Supervisor

August 23, 2017

Contents

Acronyms

DD	Diamond Difference
DG	Discontinuous Galerkin
CG	Continuous Galerkin
FE	Finite Element

Symbols

$\hat{F}$	Boundary numerical flux
$\mathbf{n}$	Normal unit vector
E	Energy
x	positional coordinate
ψ	Angular flux
$\psi^{\uparrow}$	Upwind angular flux
ϕ_g	Scalar flux of energy group g
ϕ_{lg}	l^{th} Legendre moment of the g^{th} group flux
$\mathbf{\Omega}$	Ordinate direction vector
μ	Azimuthal ordinate
η	Polar ordinate
Σ	Macroscopic cross section
H	Streaming collision operator
Q	Generic source
S	Scattering operator

Chapter 1

Introduction

Commonly when dealing with the spatial discretization of the transport equation an explicit finite differencing scheme is employed. An explicit differencing formulation allows one to "sweep" through the mesh computing the flux by utilizing previously computed flux values (or boundary values) in the trailing nodes to project the flux to the node ahead. In computation time this strategy scales linearly with the number of nodes. This is predominately why differencing schemes are still commonly employed to resolve the spatial dependence of the flux in the transport equation. While finite differencing is ideal for 1D geometries, in multidimensional problems differencing schemes are difficult to extend to irregular meshes. The simplest codes are limited to rectilinear meshes, representing the geometry with squares and rectangular regions only. This leads to poor capture of curved or organically shaped edges unless one very finely meshes the regions around such geometric features. It is possible to construct a differencing scheme for arbitrary non rectilinear meshes, but it would require pre-computing a "sweep map" which determines the node order in which the mesh is swept such that the stability of the method is preserved. In addition the differencing equations themselves become slightly more cumbersome to generate as the nodes are no longer at right angles to each other.

Other spatial discretization techniques are well suited for irregular meshes. Common strategies for discretizing PDE's on irregular meshes are the finite volume and the finite element techniques. We will focus on the finite element method in this work. Specifically, this work involves the application of discontinuous finite elements to the linear, first order radiation transport equation.

The Discontinuous Galerkin (DG) method was introduced by Reed and Hill (1973) to approximate the solution of hyperbolic PDEs [1]. One of the first applications of the method was to the radiation transport equation [2]. The DG method was later extended

to elliptic and parabolic equations [3]. Today, DG methods are extraordinarily pervasive in the numerical and applied mathematics communities. DG's popularity is due to the compact nature of the discretization scheme allowing for excellent scaling on many CPUs and due to ease of increasing the order of accuracy of the solution approximation over an element. It also allows one to tailor the coupling between neighboring elements by adjusting the so-called numerical flux which conveys information about the transport of the conserved quantity across cell boundaries.

Since the solution approximation afforded by the DG method does not enforce continuity at element boundaries it is possible to capture sharp discontinuities in the field of interest naturally. This property is important for radiation transport problems in which the flux jumps across extremely thin highly absorptive coatings; Such is the case in simulations of IFBA fuel.

It is also worth mentioning that this work is an extension of the methods introduced in the computational methods in radiation transport graduate course offered at the University of Texas at Austin. The theory and consequences of applying the discrete ordinate treatment to the angular dependence and the multigroup approximation of the energy dependence is left to the bulk of the course material. The text: Computational Methods of Neutron Transport by E.E. Lewis [4] covers these basics in detail as well.

Chapter 2

Theory

This work demonstrates the application of the discontinuities galerkin finite elements (DGFE) to the radiation transport equation in 1D. This work can be extended to two or three dimensions however, the core concepts of the DG method are readily conveyed by the 1D case.

2.1 Background

We begin by considering the time-independent, single dimensional, non-multiplying fixed source neutron transport equation given by equation 2.1. This equation is continuous in energy, space and angle.

$$\begin{aligned}\left[\Omega \cdot \nabla + \Sigma_t - \int_{E'} dE' \int_{\mathbf{\Omega}'} d\mathbf{\Omega}' \Sigma_s \left(x, E' \rightarrow E, \mathbf{\Omega}' \cdot \mathbf{\Omega}\right)\right] \psi(x, \mathbf{\Omega}, E) \\ = Q(x, \mathbf{\Omega}, E)\end{aligned} \tag{2.1}$$

Σ_t is the total macroscopic cross section. Q is an arbitrary non-fission volumetric neutron source. $\Sigma_s \left(x, E' \rightarrow E, \mathbf{\Omega}' \cdot \mathbf{\Omega}\right)$ is sometimes called the differential scattering cross section. This describes the probability per unit length of scattering from E' to the infinitesimal energy window dE about E in coincidence with scattering from angle $\mathbf{\Omega}'$ into the infinitesimal solid angle cone $d\mathbf{\Omega}$ about $\mathbf{\Omega}$. Note the differential cross section depends on the dot product between the incomming and outgoing scattering angles.

Equation 2.2 is referred to as the streaming-collision operator. This operates on the angular dependent flux, ψ, and concisely conveys the redistribution of neutrons in space

due to non-fission neutron interactions with matter.

$$H = [\Omega \cdot \nabla + \Sigma_t] \tag{2.2}$$

The scattering operator, S is given by equation 2.3 and governs the redistribution of neutrons in angle and energy due to scattering interactions.

$$S = \left[\int_{E'} dE' \int_{\mathbf{\Omega}'} d\mathbf{\Omega}' \Sigma_s \left(x, E' \rightarrow E, \mathbf{\Omega}' \cdot \mathbf{\Omega} \right) \right] \tag{2.3}$$

We can concisely write the transport equation in operator notation in equation 2.4.

$$H\psi = S\psi + Q \tag{2.4}$$

$H - S$ is sometimes defined to be the transport operator.

The next step is to apply the discrete ordinate approximation in angle and the multigroup approximation in energy. In this case, we restrict the neutrons to travel in a finite (and typically small) number, G, of energy groups. Neutrons in group g are said to have some energy on the interval $(E_g, E_{g-1}]$. The continuous energy integral in 2.1 can be replaced by the sum shown in equation 2.5.

$$\int_0^\infty dE' \approx \sum_{g'=1}^{G} \int_{E_{g'-1}}^{E_{g'}} dE' \tag{2.5}$$

Before applying the multigroup approximation to 2.1, it is advantageous to replace the differential scattering operator with a spherical harmonic series expansion. This is done to eliminate the angular dependence of the cross sections. Most numerical treatments of neutron transport do not use angular dependant cross sections and instead capture the angular redistribution action of the scattering operator through, typically, a Legendre expansion [4], (pg. 36).

$$S\psi \approx$$
$$\textstyle\sum_{l=0}^{N} (2l+1) \int dE' \Sigma_{sl}(x, E' \rightarrow E) \int d\mathbf{\Omega}' P_l(\mathbf{\Omega} \cdot \mathbf{\Omega}')\psi \tag{2.6}$$

Where l is the Legendre polynomial (P_l) order and N is the maximum number of terms to retain in the expansion. We see that the angular dependence has been eliminated from

the scattering cross section Σ_s. The Legendre addition theorem provides the identity:

$$P_l(\mathbf{\Omega} \cdot \mathbf{\Omega}') = \frac{1}{2l+1} \sum_{m=-l}^{l} Y_{lm}^*(\mathbf{\Omega}) Y_{lm}(\mathbf{\Omega}') \tag{2.7}$$

Where Y_{lm} is the spherical harmonic of degree l and order m. $*$ represents the complex conjugate. Applying 2.7 to 2.6 produces 2.8.

$$S\psi \approx$$
$$\sum_{l=0}^{N} \int dE' \Sigma_{sl}(x, E' \rightarrow E) \sum_{m=-l}^{l} Y_{lm}^*(\mathbf{\Omega}) \int d\mathbf{\Omega}' Y_{lm}(\mathbf{\Omega}') \psi \tag{2.8}$$

The inner product of the spherical harmonics with the angular dependent flux over angle $\mathbf{\Omega}'$ is represented by the scalar values, $\phi_l^m(x, E)$, 2.9:

$$\int d\mathbf{\Omega}' Y_{lm}(\mathbf{\Omega}') \psi(x, \mathbf{\Omega}', E) = \phi_l^m(x, E) \tag{2.9}$$

We can rewrite 2.8 as shown in 2.10.

$$S\psi \approx$$
$$\sum_{l=0}^{N} \int dE' \Sigma_{sl}(x, E' \rightarrow E) \sum_{m=-l}^{l} Y_{lm}^*(\mathbf{\Omega}) \phi_l^m(x, E) \tag{2.10}$$

In one dimension, we are only concerned with the direction cosine with respect to the spatial coordiante axis, $\mu = \mathbf{\Omega} \cdot \mathbf{x} = cos(\theta)$, due to symmetry. Equation 2.10 reduces to equation 2.11.

$$S\psi \approx$$
$$\sum_{l=0}^{N} (2l+1) P_l(\mu) \int dE' \Sigma_{sl}(x, E' \rightarrow E) \phi_l(x, E) \tag{2.11}$$

Where ϕ_l is the l^{th} Legendre moment of the flux given by equation 2.12.

$$\phi_l(x, E) = \frac{1}{2} \int_{-1}^{1} d\mu' P_l(\mu') \psi(x, \mu', E) \tag{2.12}$$

Now we can rewrite the one dimensional transport equation (2.1) as shown in equation 2.13.

$$\mu \frac{\partial}{\partial x} \psi + \Sigma_t \psi - \sum_{l=0}^{N} (2l+1) P_l(\mu) \int dE' \Sigma_{sl}(x, E' \rightarrow E) \phi_l(x, E)$$
$$= Q(x, \mu, E) \tag{2.13}$$

Finally we apply the multigroup approximation which yields the desired *energy discretized* non-multiplying 1D transport equation 2.14 for group g.

$$\mu\frac{\partial}{\partial x}\int_g \psi dE + \int_g \Sigma_t \psi dE - \sum_{l=0}^{N}(2l+1)P_l(\mu)\sum_{g'=1}^{G}\int_g dE\int_{g'} dE'\Sigma_{sl}(x, E'\to E)\phi_l(x,E) = \int_g Q(x,\mu,E)dE \tag{2.14}$$

Where the integral $\int_g dE$ is shorthand for:

$$\int_g dE = \int_{E_{g-1}}^{E_g} dE \tag{2.15}$$

Equation 2.14 can be written more concisely as:

$$\mu\frac{\partial}{\partial x}\psi_g(x,\mu) + \Sigma_{tg}\psi_g(x,\mu) - \sum_{l=0}^{N}(2l+1)P_l(\mu)\sum_{g'=1}^{G}\Sigma_{lgg'}\phi_{lg'}(x) = Q_g(x,\mu) \tag{2.16}$$

Where $\Sigma_{lgg'}$ is the scattering kernel and is derived in E.E Lewis's text [4]. The group total cross section is given by:

$$\Sigma_{tg} = \frac{\int_g \Sigma_t(E)\phi(E)dE}{\int_g \phi(E)dE} \tag{2.17}$$

Unfortunately these group cross sections depend on already knowing the scalar flux as a function of energy. This complication is the subject of an enormous quantity of literature on neutron self-shielded cross section generation. The reader can use the program NJOY to generate approximate self shielded cross sections for a variety of assumed background spectra, if desired.

There is still an angular and spatial dependence in the energy discretized equation 2.16, therefore we apply the discrete ordinates approximation to simplify the equation further and prepare for the application of the DGFE spatial discretization technique.

The discrete ordinates approximation requires 2.16 to hold for only a few specified directions, $\mu^n \in [1,-1]$ where μ is the cosine of the ordinate direction with the x axis. Additionally, we apply a quadrature approximation to the integral term.

This deceivingly simple assumption leads to the angle and energy discretized transport equation 2.18.

$$\mu^n\frac{\partial}{\partial x}\psi_g^n(x) + \Sigma_{tg}\psi_g^n(x) = \sum_{l=0}^{L}(2l+1)P_l(\mu^n)\sum_{g'\neq g}^{G}\Sigma_{lgg'}\phi_{lg'}(x) + Q(x) \tag{2.18}$$

The superscript n denotes a fixed ordinate index rather than an exponent. $\phi_{lg'}(x)$ are the Legendre moments of the flux computed by a simple quadrature rule given by equation 2.19.

$$\phi_{lg'}(x) = \frac{1}{2}\sum_{n=1}^{N} w_n P_l(\mu^n)\psi_{g'}^n(x) \tag{2.19}$$

The weights w_n are typically computed using a level-symmetric or Gauss-Legendre quadrature rule and can be found in [4]. N is the number of ordinate directions to track.

Equation 2.18 be rewritten simply as:

$$\mu^n \frac{\partial}{\partial x}\psi_g^n(x) + \Sigma_{tg}\psi_g^n(x) = S(x) + Q(x) \tag{2.20}$$

Where $S(x)$ is the scattering source term from all other energy groups $g' \neq g$ and from all other angles $\mu_n' \neq \mu_n$. We will take the volumetric source , Q to be zero in the following work.

Though this transport equation holds only for the extreemly limited case of a steady-state non multiplying medium in one-dimension, it provides a useful starting point to investigate the spatial discretization of the neutron flux. As previously stated, we focus on the DGFE approach here.

2.2 DGFE Theory

We begin with equation 2.20; the within group g, within angle n 1D transport equation. In the following section we drop the group subscript and angle superscript and set $Q(x) = 0$.

$$\mu \frac{\partial}{\partial x}\psi(x) + \Sigma_t\psi(x) = S(x) \tag{2.21}$$

Equation 2.21 is a first order, linear, ordinary differential equation, as such the methods introduced in chapter 6 (even parity transport) of E. E. Lewis's computational methods in radiation transport largely do not apply. The even parity formulation of the transport equation contains a spatial derivative of order 2 results in certain nice aspects to the DGFE discretized equations – primarily that even order equations yield symmetric matrices after discretization. The even parity formulation of the transport equation is not pursued here since it has difficulty including anisotropic scatter [4]. It is possible to use the Petrov-Galerkin method on the first order equation without constructing the second order form of the transport equation.

First, we multiply both sides of equation 2.21 by a yet to be defined test function,

$v(x)$ resulting in:

$$\mu\frac{\partial}{\partial x}\psi(x)v(x) + \Sigma_t\psi(x)v(x) = S(x)v(x) \tag{2.22}$$

Next the equation is integrated over the domain, $x \in [0, L]$:

$$\int_0^L \mu\frac{\partial\psi(x)}{\partial x}v(x)dx + \int_0^L \Sigma_t\psi(x)v(x)dx = \int_0^L S(x)v(x)dx \tag{2.23}$$

This is known as the weak form of equation 2.21.

Next, we integrate the first term in 2.23 by parts giving:

$$\mu\psi(x)v(x)|_0^L - \mu\int_0^L \psi(x)\frac{\partial v(x)}{\partial x}dx + \int_0^L \Sigma_t\psi(x)v(x)dx = \int_0^L S(x)v(x)dx \tag{2.24}$$

We are free to choose a functional form for $v(x)$. In the Galerkin approach, the test function is taken to be of the same functional form as the solution approximation $\psi(x)$. The simple DGFE choice is to take $v(x)$ to be a linear combination of ramp functions. Each ramp function $h_{ei}(x)$ is supported only at one nodal location in the mesh and is defined to be zero at all other nodes. Figure 2.1 displays two interior neighboring ramp functions which are each non-zero over element e_1. The ramp functions are defined to have unit height over their supporting node. An element is defined to be the region between bounding nodes which are points at which the solution is supported. For simplicity all elements are assumed to have width Δx.

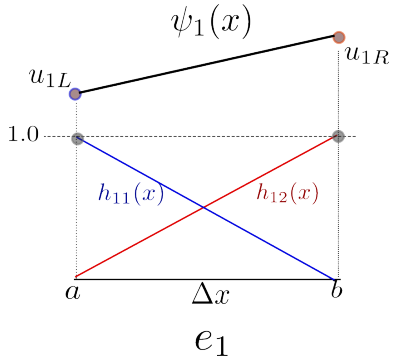

Figure 2.1: Single finite element.

In practice the transport equation is integrated element-by-element, rather than over the whole domain. The contribution of each element will be summed together to recover the neutron balance over the whole domain. For now, we consider an interior element, e_1 defined on the sub-region: $[a, b]$. Figure 2.2 shows the interior element e_1 bounded by two other elements. Note that the hypothetical DGFE numerical solution ψ jumps

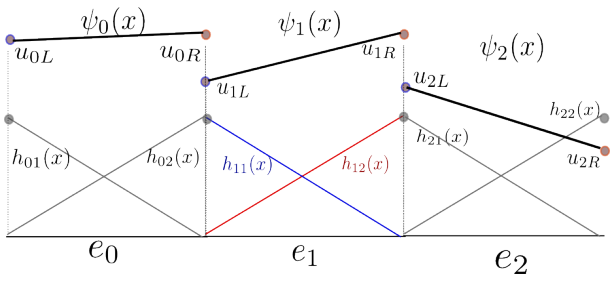

Figure 2.2: Multiple DG finite elements.

in value at element boundaries. As a consequence, at element boundaries the solution is double valued at mesh edges. This is where the Discontinuous Galerkin finite element scheme differs from the more commonly known Continuous Galerkin (CG) FE spatial discretization method.

Now it is useful to formally define the ramp functions and their linear combination. Over a single element, the solution $\psi_e(x)$ is given by equation 2.25.

$$\psi_e(x) = u_{eL}h_{e1}(x) + u_{eR}h_{e2}(x) = \sum_i u_{ei}h_{ei}(x), \;\; x \in [a, b] \tag{2.25}$$

Where i is the edge index, in the one dimension case this denotes either the left or right face. The ramp functions are given as:

$$h_{e1}(x) = \begin{cases} \frac{-1}{\Delta x}(x - a) + 1 & , x \in [a, b] \\ 0 & , otherwise \end{cases} \tag{2.26}$$

and

$$h_{e2}(x) = \begin{cases} \frac{1}{\Delta x}(x - a) & , x \in [a, b] \\ 0 & , otherwise \end{cases} \tag{2.27}$$

As previously stated, the Galerkin approach is to enforce 2.28.

$$\psi_e(x) = v_e(x) \tag{2.28}$$

on each element. At first glance this appears this is an arbitrary choice, and indeed, this assumption does not have to be made. One could use different functional families for ψ and v, however we will not investigate this option.

For this case where we have chosen simple ramp functions to represent our 1D solution approximation, each element has two unknown scalar values, $\{u_{eL}, u_{eR}\}$ that act to scale the ramp functions over the element.

$$\mu\psi_e(x)v_e(x)|_a^b - \mu\int_a^b \psi_e(x)\frac{\partial v_e(x)}{\partial x}dx + \int_a^b \Sigma_t\psi_e(x)v_e(x)dx = \int_a^b S_e(x)v_e(x)dx \quad (2.29)$$

Next we apply 2.25 and 2.28 to 2.29. The solution over the entire domain is the summation of the piecewise linear solution approximation over all elements:

$$\psi(x) = \sum_{e=0}^{M}\psi_e(x) \quad (2.30)$$

Where M is the number of finite elements used.

The integral terms in equation 2.29 can be expanded to explicitly show their dependence on the scaling factors. The second term in 2.29 integrates to 2.31.

$$W_e = -\int_a^b \mu\psi_e\frac{\partial v_e}{\partial x}dx = \frac{-\mu}{2}(u_{eR}^2 - u_{eL}^2) = \frac{-\mu}{2}\mathbf{u}_e\begin{bmatrix}-1 & 1\\ -1 & 1\end{bmatrix}\mathbf{u}_e^T \quad (2.31)$$

With $\mathbf{u}_e = [u_{eL}, u_{eR}]$. Note that this produces an asymmetric element matrix. As a consequence, it is required that the order of the nodes from left to right is preserved.

The third term in 2.29 integrates to 2.32.

$$M_e = \int_a^b \Sigma_t\psi_e(x)v_e(x)dx = \frac{\Sigma_t\Delta x}{3}(u_L^2 + u_Lu_R + u_R^2) = \frac{\Sigma_t\Delta x}{3}\mathbf{u}_e\begin{bmatrix}1 & 1/2\\ 1/2 & 1\end{bmatrix}\mathbf{u}_e^T \quad (2.32)$$

The RHS of equation 2.29 integrates to 2.33.

$$RHS_e = \int_a^b S_e(x)v_e(x)dx = \frac{S_e\Delta x}{2}(u_L + u_R) = \frac{S_e\Delta x}{2}\begin{bmatrix}1\\ 1\end{bmatrix}\mathbf{u}_e^T \quad (2.33)$$

Where we take the value S_e to be the value of $S_e(x)$ at the element mid-point. This is valid provided that $S_e(x)$ is a linear function since this is equal to the average value of $S_e(x)$ over the element.

Finally, we must deal with the boundary term which arose from integrating the first term of equation 2.29 by parts. This term is the only term which will contain information from neighboring elements in its definition. This is why it is said that the DGFE technique is "compact". Let the outward normal at a given element boundary to be denoted by $\mathbf{n}$. The left side outward normal for element e_1 is depicted in figure 2.3.

It is useful to define a jump and average condition on an element boundary. The

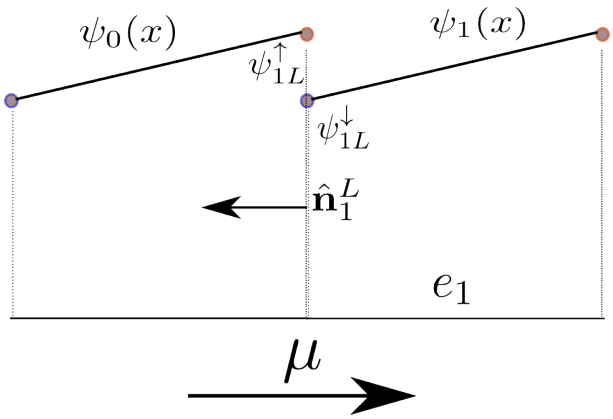

Figure 2.3: Outward normal on left face of element e_1. As drawn, $\psi_{1L}^{\uparrow} = u_{e_0,2}$ and $\psi_{1L}^{\downarrow} = u_{e_1,1}$ in the figure.

average condition at the junction between two elements is given by 2.34.

$$\{\{u\}\}_p = \frac{1}{2}(\lim_{x\to p^+} \psi(x) + \lim_{x\to p^-} \psi(x)) \tag{2.34}$$

Where the subscript p denotes evaluation at a boundary. Since $\psi(x)|_p$ and therefore u_p is double valued at the element boundaries; the limit approaching from the left is not equal to the limit approaching from the right.

And the jump is provided by equation 2.35.

$$[[u]]_p = (\lim_{x\to p^+} \psi(x) - \lim_{x\to p^-} \psi(x)) \tag{2.35}$$

Now it is useful define the "upwind" flux. According to 2.36, the sign of the dot product between the current neutron flow direction, μ and the boundary normal vector $\mathbf{n}_{e,p}$ can be used at each edge to determine the upwind flux value.

$$\psi^{\uparrow} = \begin{cases} \psi_k|_p & \text{if } \mu \cdot \mathbf{n}_e|_p \leq 0 \\ \psi_e|_p & \text{if } \mu \cdot \mathbf{n}_e|_p > 0 \end{cases} \tag{2.36}$$

Where k represents the neighboring element and e is the current element.

It is unclear what value to choose for the flux at the element boundaries. This is required to evaluate $\mu\psi_e(x)v_e(x)|_a^b$ in 2.29. The DGFE method introduces the numerical flux $\mu \cdot \mathbf{n}\hat{F}$ to resolve this issue. The boundary term becomes 2.37.

$$\mu\psi_e(x)v_e(x)|_a^b = \mu \cdot \mathbf{n}\hat{F}v_e(x)|_a^b \tag{2.37}$$

Upwind Formulation

In this case, when evaluating $\mu\psi_e(x)v(x)|_a^b$, $\psi(x)$ always takes the upwind value at element boundaries.

$$\mu \cdot \mathbf{n}\hat{F} = \mu \cdot \mathbf{n}\psi^{\uparrow} \tag{2.38}$$

This makes physical sense if the neutrons are constrained to flow in the direction μ by the discrete ordinates approximation. The value of angular dependent neutron flux at the element boundaries should depend only on the neutron's behavior immediately upstream of the boundary. In other words, all neutron interactions downstream of the boundary do not have a large influence on the upstream flux. This is true particularly in the case of the once-collided flux. It was not discussed in this work, but equation 2.23 is written for a single scattering source iteration (SI). For more information on source iteration, see E.E. Lewis's text [4].

Equation 2.37 can now be evaluated. If $\mu \cdot \mathbf{n} > 0$:

$$B_{ep_1} = \mu \cdot \hat{\mathbf{n}}\hat{F}v(x)|_{p_1} = \mu \cdot \mathbf{n}(u_e^2)|_p = (\mu \cdot \mathbf{n})\mathbf{u}_p \begin{bmatrix} 1 & 0 \\ 0 & 0 \end{bmatrix} \mathbf{u}_p^T \tag{2.39}$$

Where $\mathbf{u}_p = [u_e, u_k]|_p$. Again, $u_k|_p$ is the value of ψ as the boundary from the neighboring element side (i.e $u_k = \lim_{x \to p^k} \psi(x)$) and likewise for the current element side: $u_e|_p = \lim_{x \to p^e} \psi(x)$.

If $\mu \cdot \mathbf{n} \leq 0$:

$$B_{ep_2} = \mu \cdot \hat{\mathbf{n}}\hat{F}v(x)|_{p_2} = \mu \cdot \mathbf{n}(u_e \cdot u_k)|_p = (\mu \cdot \mathbf{n})\mathbf{u}_p \begin{bmatrix} 0 & 0 \\ 1 & 0 \end{bmatrix} \mathbf{u}_p^T \tag{2.40}$$

And the sum over both edges is given by 2.41.

$$B_{ep_1} + B_{ep_2} = \mu \cdot \hat{\mathbf{n}}\hat{F}v(x)|_a^b \tag{2.41}$$

Average Flux Formulation

Alternatively, instead of simply taking the upwind flux value at each element boundary, one may choose to use the average flux, $\{\{u\}\}_p$ at each boundary. This results in the following:

If $\mu \cdot \mathbf{n} \leq 0$:

$$B_{ep_1} = \mu \cdot \hat{\mathbf{n}} \hat{F} v(x)|_{p_1} = \mu \cdot \mathbf{n} \frac{u_e}{2} (u_e + u_k)|_p = (\mu \cdot \mathbf{n}) \mathbf{u}_p \begin{bmatrix} 1/2 & 0 \\ 1/2 & 0 \end{bmatrix} \mathbf{u}_p^T \tag{2.42}$$

and If $\mu \cdot \mathbf{n} > 0$:

$$B_{ep_2} = \mu \cdot \hat{\mathbf{n}} \hat{F} v(x)|_{p_2} = \mu \cdot \mathbf{n} \frac{u_e}{2} (u_e + u_k)|_p = (\mu \cdot \mathbf{n}) \mathbf{u}_p \begin{bmatrix} 1/2 & 0 \\ 1/2 & 0 \end{bmatrix} \mathbf{u}_p^T \tag{2.43}$$

This formulation makes physical sense in the case that upstream and downstream interactions influence the value of the flux at element boundaries. In the purely diffusive case, where Fick's law holds, this assumption is valid an therefore the average flux is a good choice. In the case of the hyperbolic first order equation 2.23, the average boundary flux formulation might lead to unphysical results.

System Matrix Construction and Boundary Conditions

For each element in the mesh we can write the neutron balance as:

$$B_{ep_1} + B_{ep_2} + W_e + M_e = S_e \tag{2.44}$$

Multiplying both sides by $[\mathbf{uI}]^{-1}$ we obtain:

$$[b_{ep_1} + b_{ep_2} + w_e + m_e]\mathbf{u}^T = s_e \tag{2.45}$$

Where $w_e = [\mathbf{uI}]^{-1} W_e$, $s_e = [\mathbf{uI}]^{-1} S_e$, and $m_e = [\mathbf{uI}]^{-1} M_e$ and $\mathbf{I}$ is the identity matrix. Collapsing further:

$$[A_e]\mathbf{u}^T = s_e \tag{2.46}$$

The goal is to find the combination of the scaling factors, $\mathbf{u} = \{u_0, u_1, ...\}$, over all elements that best satisfies the overall weak form of the neutron balance equation 2.23. One can think of the finite element method in an optimization context in which some (hopefully unique) combination of the scalars $\mathbf{u} = \{u_0, u_1, ...\}$ reduces the residual of 2.23 to some minimal value.

To assemble the system matrix $\mathbf{A}$, the individual element matrices are "stamped" into $\mathbf{A}$. Since each node in the mesh is assigned a *unique ID* the elements of A_e can be copied into the global matrix $\mathbf{A}$.

After $\mathbf{A}$ is constructed, the discretized, non-multiplying transport equation can be

written as:

$$\mathbf{A}\mathbf{u}^T = \mathbf{s} \tag{2.47}$$

$\mathbf{A}$ is a sparse, non symmetric matrix. This linear system of equations can be solved by GMRES or other iterative techniques.

Up until this point we have disregarded the application of boundary conditions since we focused on the interior elements. For the first order transport equation, all boundary conditions (vacuum, reflective, white) can be described as either fixed or free. A Fixed boundary condition specifies the value of ψ at the boundary. This arises in the vacuum case where inward facing ordinate fluxes are set equal to zero at the boundary. This also arises in the reflective and white cases where the banked outward fluxes from the previous scattering source iteration are assigned as fixed boundary values for the inward facing ordinate fluxes. A free boundary arises in cases where the flux is allowed to escape from the domain. To implement a fixed boundary condition, the row in the global system matrix, A, corresponding to the boundary node is set equal to zero at all elements except at the diagonal where the diagonal entry is set equal to 1. On the right hand side the specified value for the flux at that node is set. Free boundary conditions require no action.

Chapter 3

Results

In all cases the group structure boundaries of:

$$[1.\text{E-}3, 1.\text{E-}2, 1.\text{E-}1, 1.E0, 1.E1, 1.E2, 1.E3, 1.E4, 1.E5, 1.E6, 1.E7](eV)$$

were used to generate a 10-group cross section library. The infinite dilution multigroup cross sections were generated with NJOY for this work [5]. For plotting, the group scalar fluxes are recovered from the angle-dependant flux by the quadrature rule:

$$\phi_g = \frac{1}{2}\sum_{n=1}^{N} w_n \psi_g^n(x) \tag{3.1}$$

For all presented results, S_8 Gauss-Legendre quadrature was used for the angular flux decomposition by the discrete ordinates method. Accordingly, the scattering cross section was approximated with the first 8 Legendre moments (thus retaining the first 8 terms in the Legendre expansion of the scattering kernel). For consistency, all cases were executed with 160 scattering source iterations to converge the angle and energy neutron distribution.

The first result shown in figure 3.1 demonstrates the discontinuous nature of the solution approximation. Neutrons are introduce traveling from left to right with an initial energy of $1e7eV$ and with a source flux of $1.27E6[n/cm^2s]$ into a 50cm thick graphite block. The upwind formulation was used for the numerical flux. The graphite was pure ^{12}C with a density of $2.23[g/cc]$. The case was executed using a relatively coarse 20 element spatial mesh for visual clarity of the discontinuities.

The same problem was re-run this time with the average numerical flux formulation. This resulted in figure 3.2.

Interestingly, for this problem it appears the upwind strategy provides a more accurate

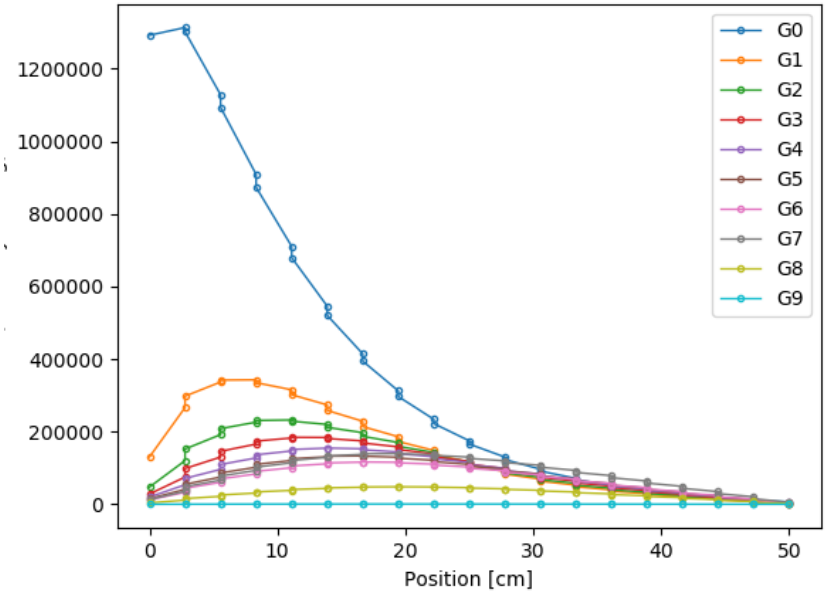

Figure 3.1: Group scalar fluxes for a high energy beam incident on a graphite block. The y axis units are in n/cm^2s. Upwind numerical flux used.

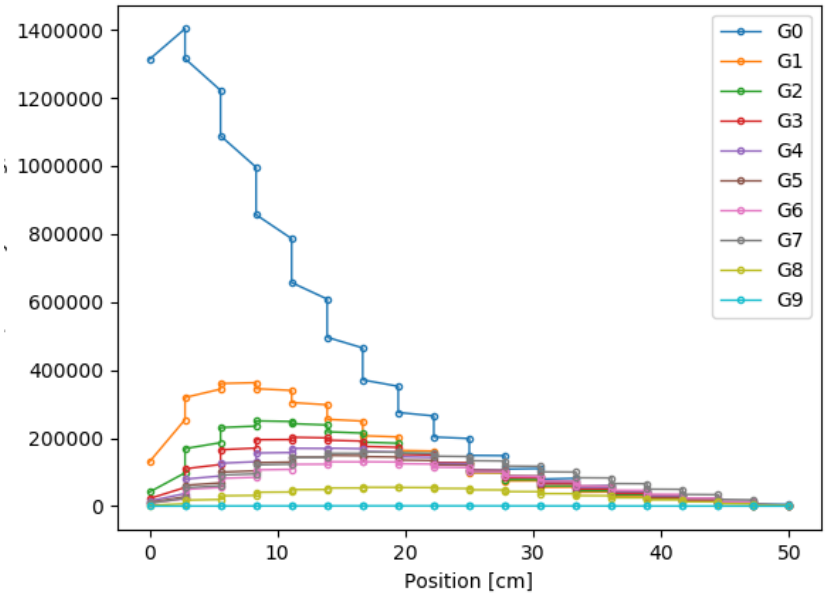

Figure 3.2: Group scalar fluxes for a high energy beam incident on a graphite block. The y axis units are in n/cm^2s. Average numerical flux used at element boundaries.

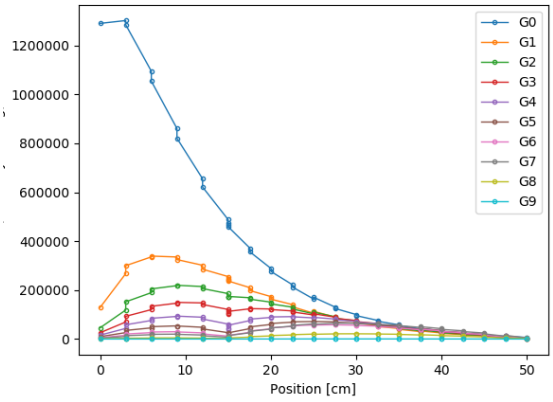

Figure 3.3: Coarse mesh solution of the graphite block with a ^{10}B sheet at 15$[cm]$.

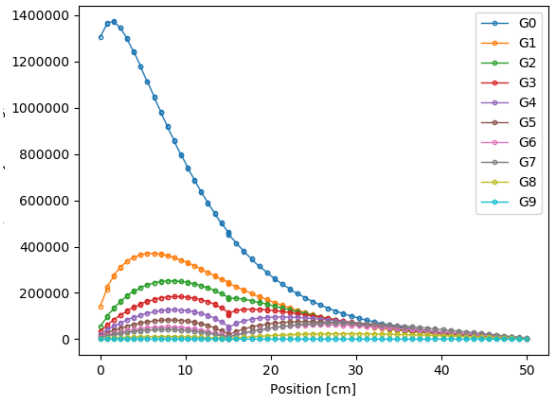

Figure 3.4: Fine mesh solution.

result. Qualitatively, the expected far-field exponential decay of the highest energy group flux is more accurately captured by the upwind flux formulation.

In the next case, a thin (0.5$[mm]$) sheet of highly absorptive pure ^{10}B with a density of 5$[g/cc]$ was inserted into the graphite block at 15$[cm]$. Shown in figure 3.3, this effectively eliminated the majority of the thermal neutron current passing through the region resulting in a sharp dip in thermal flux near the sheet, followed by thermal neutron recovery further away since there are still neutrons down scattering into the lower energy groups over the whole domain. Expectedly, the boron had little influence on the higher energy groups. The first case was executed with 20 elements followed by a fine mesh run with 60 elements.

Chapter 4

Conclusion

The DGFE method was introduced and implemented in 1D. The current implementation could serve as a starting point to more detailed investigations stated below.

It was shown that DGFE allows for a flexible definition of the numerical flux and that this choice has a significant impact on the resulting numerical approximation.

In the case of a thin absorbing boron region in a graphite block, sharp changes in the flux were captured.

A mesh convergence study could be performed in the future to experimentally determine the spatial order of convergence of the DGFE scheme. Additionally, the results could be benchmarked against gold-standard monte-carlo simulations to ascertain the accuracy of the method, particularly when thin absorptive regions are present in the domain.

Improving the order of accuracy of the finite element discretization is a potential avenue for future work. This would involve increasing the polynomial order of the ramp basis functions over each element from 1 to 2. Future studies could also investigate parallelization strategies. In some respects, it is easy to parallelize the spatial transport solve because each angle and energy independent $\mathbf{A}\mathbf{u}^T = \mathbf{s}$ system can be solved independently. In addition, the scattering source can be updated in each element independently.

It has been shown that the DGFE method "locks" in the optically thick diffusion limit, meaning, the flux is artificially depressed in regions that are highly opaque and highly diffusive to neutrons. For most practical problems this is not a concern, however, it could be interesting to investigate the work performed by J. Guermond et. al (2014) [6] on this subject. Guermond et. al. present a method to adaptively choose between the unwinding and averaging formulation in each element independently based on the local scattering cross section and cell width. This has been shown to effectively eliminate this issue with the DGFE method without significant additional computational overhead.

The code is available online at https://github.com/wgurecky/spyTran.

Bibliography

[1] P. Lesaint and P. Raviart. On a finite element method for solving the neutron transport equation. *Mathmatical Aspects of Finite Elements in Partial Differential Equations*, 33, 1974.

[2] W. Reed and T. Hill. Triangular mesh methods for the neutron transport equation. *Los Alamos National Lab*, LA-UR-73-479, 1973.

[3] B. Riviere. Discontinuous galerkin method for solving elliptic and parabolic equations: Theory and implementation. *SIAM Frontiers in Applied Mathematics*, 2008.

[4] Lewis E. *Numerical Methods for Radiation Transport*. CRC Press, 2015.

[5] R. Macfarlane et al. The njoy nuclear data processing system. *Los Alamos National Laboratory (LANL)*, LA-UR-17-20093, 2017.

[6] Jean-Luc Guermond, Guido Kanschat, and Jean C. Ragusa. *Discontinuous Galerkin for the Radiative Transport Equation*, pages 181–193. Springer International Publishing, Cham, 2014.